Suppression of the sidewall effect in pillar array columns with radially elongated pillars

Jeff Op De Beeck[a], Manly Callewaert[a,b], Heidi Ottevaere[b], Han Gardeniers[c], Gert Desmet[a], Wim De Malsche[a,*]

[a] Department of Chemical Engineering, Vrije Universiteit Brussel, Pleinlaan 2, 1050 Brussels, Belgium
[b] B-PHOT, Department of Applied Physics, Vrije Universiteit Brussel, Pleinlaan 2, 1050 Brussels, Belgium
[c] Mesoscale Chemical Systems, Mesa+ Institute for Nanotechnology, P.O. Box 217, 7500AE Enschede, The Netherlands

ARTICLE INFO

ABSTRACT

An important bottleneck of pillar array columns designed for liquid chromatography is that small deviations of the target 'magical distance' at the sidewall region leads to detrimental sidewall effects, due to local differences of linear velocities at the sidewall region versus other locations in the pillar bed. In the present study, we demonstrate that a lateral elongation of the pillar significantly increases the tolerance for offsets of the magical distance. By shifting the sidewall distance 600 nm for 2 pillar aspect ratio (AR) designs (AR = 3 and 9), only minor sidewall effects on the measured plate heights could be observed for the AR = 9 columns, while the plate height was roughly doubled when using the wrong versus the correct sidewall distance for the AR = 3 columns. Technologically, this constitutes a huge advantage because small deviations (order of 100 nm) between the set and the finally achieved value for the inter-pillar distance are very common using mid-UV lithography based etching processes.

© 2014 Elsevier B.V. All rights reserved.

1. Introduction

Pillar array columns (PACs) have been studied rather intensively during the last decade as a new support in liquid chromatography [1–10]. The main advantage of PACs is that they offer a dramatic reduction of the eddy-dispersion because the photo-lithographic etching techniques with which they are fabricated, enables to produce beds consisting of perfectly repeated and uniform unit cells. Their potential has been demonstrated by computational fluid dynamics simulations as well as by experimental characterization. However, an important limitation of PACs is the occurrence of the so-called sidewall effect. [4,11,12]. While the structural order of PACs is a crucial element of their improved performance, the fact that they need to be enclosed by a containing wall however also inevitably distorts the shape of the PACs at the pillar layer most close to the sidewall of the array. Due to the perfect order, this distortion persists all along the length of the bed. This inevitably leads to a persisting difference in flow resistance between these two outer layers and the rest of the bed. As a consequence, the bands either persistently lag or lead near the sidewall. Because of the ongoing radial dispersion, it gradually affects the entire column cross-section, eventually consuming most of the available separation efficiency [4].

The theoretically best way to overcome this sidewall problem is by changing the width of the through-pore immediately adjacent to the sidewall such that the flow resistance near the sidewall is the same as in the through-pores in the rest of the bed. Theoretical calculations have shown that, for the case of a bed of cylindrical pillars, the flow resistances can be completely equalized when the distance between the (straight) sidewall and the nearest pillars (5 μm diameter, 40% porosity) is 750 nm [11]. However, the same calculations also revealed that a small deviation from this rule can lead to a dramatic increase of the dispersion again (5% deviation, corresponding to a 250 nm error can lead to an increase of the plate height with 0.7 reduced plate height uses). This extreme sensitivity raises a severe challenge for the fabrication of PACs, because the dimensions of the etched pillars inevitably undergo a deviation of a few 10 nm to several 100 nm during the transformation of the mask design to the actual microfabricated device. Unfortunately, this deviation usually has the biggest effect on the pillar spacing at the sidewall, as this is usually the smallest dimension in the column. Having only access to mid-UV lithography, as most universities and research institutes, [13,14], this sidewall effect is in fact the main reason why most of the recent work of our group focused mainly on columns with

---

a relatively large inter-pillar spacing (mostly 2.5 μm), because the replication of the mask is always better for larger features (applying a given wavelength during lithography).

Very recently, our group has also proposed the use of radially elongated pillars (REP's) as a means to reduce B term dispersion and the footprint of the channel [15]. Defining a pillar aspect ratio AR as the ratio of the radial over the axial pillar width (see Fig. 1), it was demonstrated that a fivefold reduction of the minimal plate height could be obtained by moving from a bed with radially elongated pillars with an AR close to unity (AR = 1.2) to a bed with AR = 15, while keeping the same inter-pillar distance. During that study, it was noticed that the bands remained very straight, also close to the sidewall, despite the fact that no efforts had been made to optimize the sidewall region. In the present contribution, this effect is studied in detail, by comparing PACs with two different sidewall distances (SWD = 2.0 μm and SWD = 2.6 μm) and with two degrees of radial pillar elongation (resp. aspect ratio AR = 3 and 9), giving in total 4 combinations to be tested (see Figs. 1a–d).

2. Experimental

2.1. Sample and coating

The dyes Coumarin C440 (Cas no. 26093-31-2, Sigma–Aldrich, Belgium), and C480 (Cas no. 41267-76-9) were dissolved in HPLC-grade methanol at a final concentration of 1×10^{-3} M, after which they were filtered. When only one coumarine was being tested, C440 was used at 0.2 mM concentration. In all other cases, the concentration was reduced by blending it with the proper water methanol mixture to a concentration of 0.40 mM, 0.20 mM for C480

and C440 respectively to obtain more or less the same intensities at the detector. A C8 hydrophobic coating was applied on the porous silica layer by means of a liquid-phase coating procedure consisting of the following steps. First, the microchannels were flushed with methanol for 1 d and anhydrous toluene for 1 d. A solution of 5% octyldimethylchlorosilane (C8) in anhydrous toluene was pumped through the channel for 72 h at room temperature. Afterwards, the channels were flushed with anhydrous toluene for 1 d and with methanol for 1 d.

2.2. Microfabrication and channel design

The pillar array columns were patterned using mid-UV photolithography (photoresist, Olin 907-12), followed by a Bosch-type deep-reactive-ion etching step (Adixen AMS100SE) up to a depth of 8 μm. Next, the through-holes were defined by mid-UV lithography from the back side (photoresist, Olin 907-35), again followed by a Bosch etching step to produce the through-holes. After this, the resist was removed by oxygen plasma and nitric acid. The microfluidic channels were subsequently sealed with a Pyrex wafer (thickness 0.5 mm), anodically bonded to the silicon using an EVG EV-501 wafer bonder (EV Group Inc., Schaerding, Austria). Next, the chip was diced. A holder was made in-house to provide the interfacing with HPLC connection pieces. The channels were 1 mm wide and 12 mm long, and were preceded by an injection box as shown at the top of Fig. 3. In each PAC, the spacing between the REP features in the bed was 3.0 μm. The axial distance between the pillars was in each case equal to 3 μm. Fig. 2 shows SEM images of two of the finally produced PACs, one with aspect ratio AR = 3 and one with AR = 9.
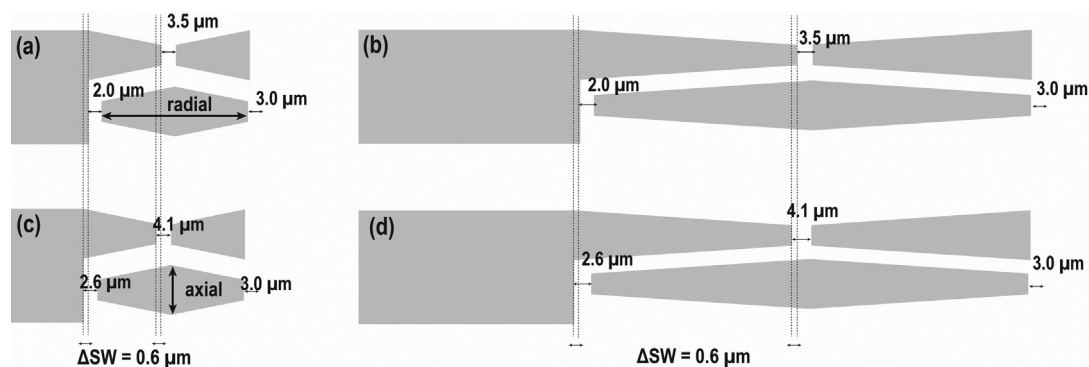

Fig. 1. Sidewall details of the masks designed the different PACs tested in the present study: (a) AR = 3 and SW-distance = 2.0 μm; (b) AR = 3 and SW-distance = 2.6 μm; (c) AR = 9 and SW-distance = 2.0 μm; (d) AR = 9 and SW-distance = 2.6 μm.
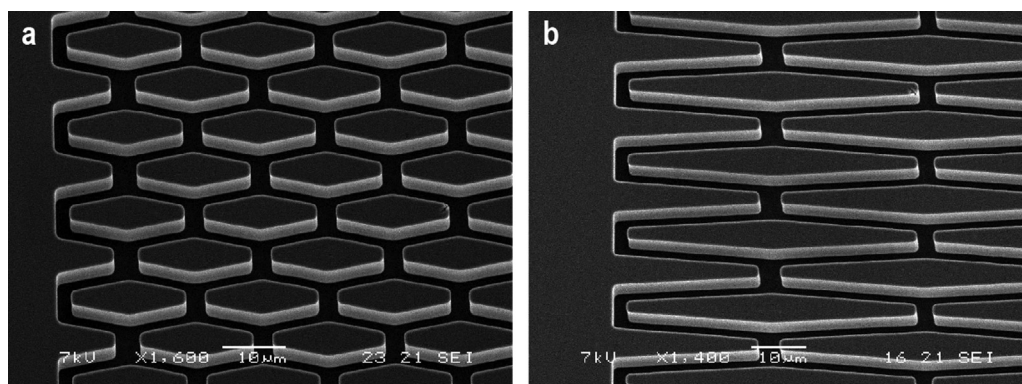

Fig. 2. SEM image of a PAC with (a) AR = 3 and (b) AR = 9. In both cases, the characteristic SW-distance was equal to 2.0 μm.
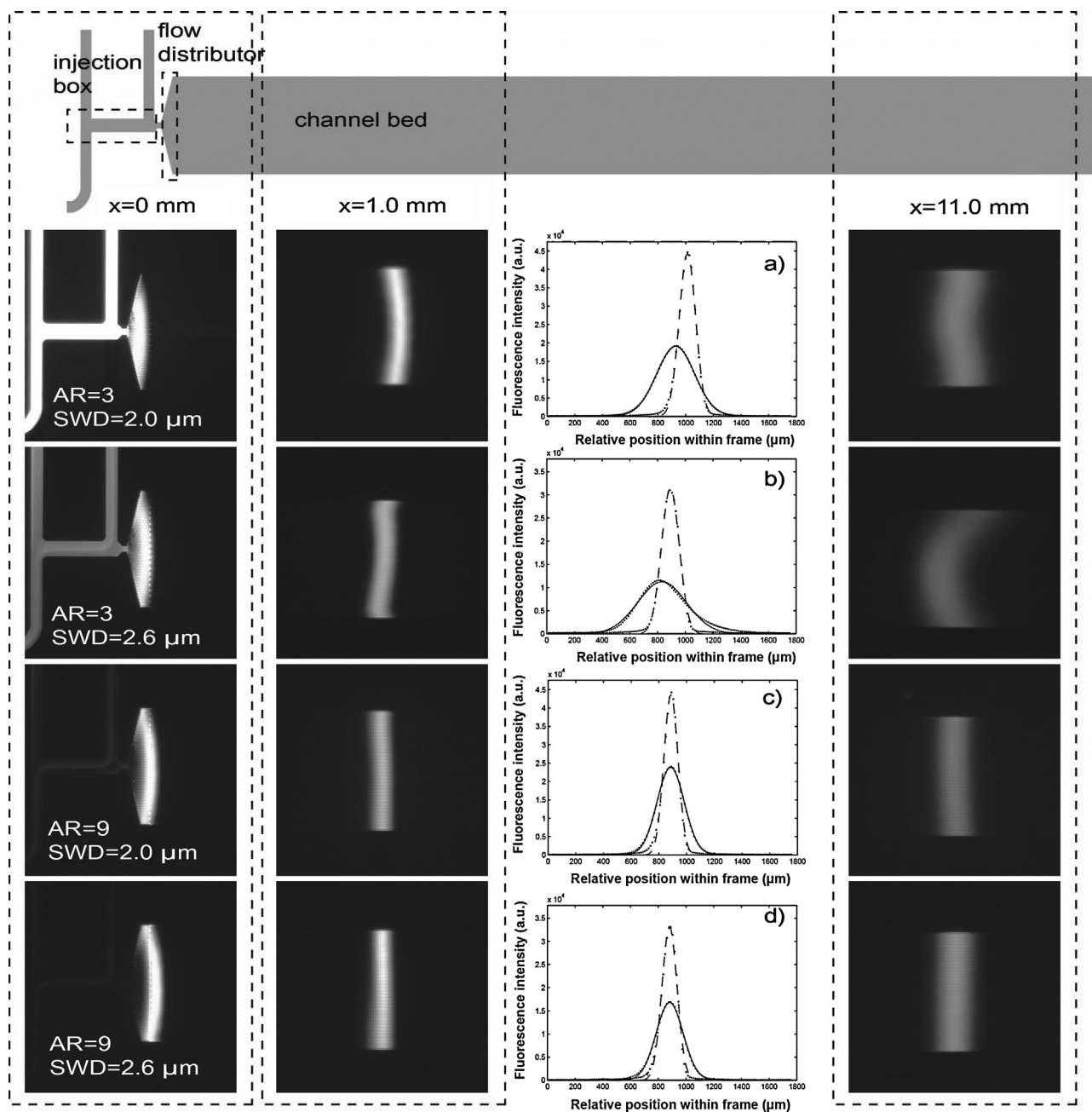
Fig. 3. General overview of the PAC geometry (top figure) showing the injection box, the flow distributor and the actual channel bed, followed by four rows of CCD camera images of coumarin C440 sample bands (both sample and mobile phase solvent was 100% methanol) at the injection zone (left), 1 mm downstream the channel inlet (middle) and 11 mm downstream the channel inlet (right) for (a) AR = 3, sidewall distance (SWD) = 2.0 μm, linear velocity 0.75 mm/s, (b) AR = 3, SWD = 2.6 μm, linear velocity 1.32 mm/s, (c) AR = 9, SWD = 2.0 μm, linear velocity 0.15 mm/s, (d) AR = 9, SWD = 2.6 μm, linear velocity 0.55 mm/s. The overlaid band profiles shown in the 3rd panel of each row represent the intensity read-outs of the bands at 1 mm (dotted line) and at 11 mm (full line).
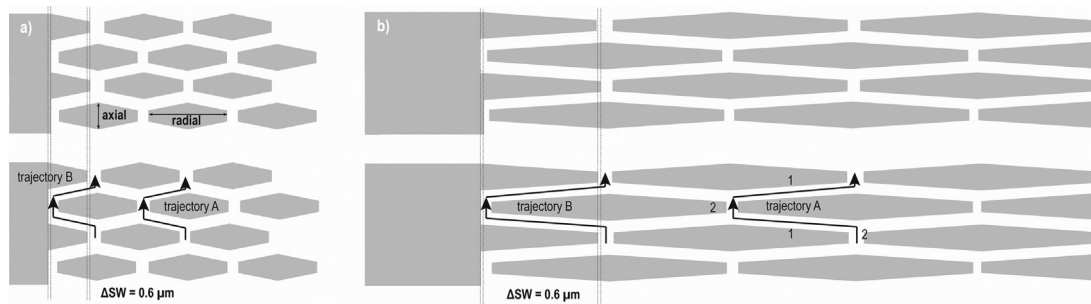

Fig. 4. Schematic overview and comparison of flow paths at sidewall and central channel regions (a) AR = 3 and (b) AR = 9.

2.3. Injection and detection

The sample injection was performed using an automated valve system, controlled with an in-house written C++ program, as already described in [4]. In brief, first the injection box is filled with sample using an in- and outflow channel, while keeping the mobile phase in- and outlet of the column closed. Subsequently, the valves are switched, such that the mobile phase pump now flows through the injection box and takes the sample into the column. For the mobile phase propagation an Agilent 1100 series nano pump (Agilent Technologies GmbH, Waldbronn, Deutschland) was used. The sample was driven into the chip using a pressurized nitrogen vessel that pushed the sample to the chip. During the sample injection step, the automated valve system ensures that the inlet and the outlet of the mobile phase circuit were closed. During the subsequent sample separation, the inlet and the outlet of the sample injection circuit were diverted to a high flow resistance capillary, allowing for the existence of a small leakage flow and thus avoiding tailing. A Hg-vapour lamp was used to excite the fluorescent dye in the UV. The peaks were visualized using an air-cooled CCD fluorescence camera (Hamamatsu Photonics K.K., Japan). The peak intensity profiles were subsequently analyzed using the accompanying Simple PCI® image analysis software. On-column chromatograms were obtained by averaging a row of pixels and plotting its values as a function of time. For the determination of the peak widths and plate heights, the peak fluorescence intensity was averaged across the channel width. The thus obtained axial concentration distribution was subsequently fitted with a Gaussian function using Sigmaplot®. The concentration profiles and the accompanying variances were determined at 11 mm downstream the injection H is then obtained as $(\sigma_{x,e}^2 - \sigma_{x,0}^2)/\Delta x$, wherein $\sigma_{x,e}$ and $\sigma_{x,0}$ are the variance of the injected band at the end and the initial position and wherein Δx is the distance between both positions.

3. Results

3.1. Visual observations

Fig. 2 shows some examples of SEM pictures taken from the sidewall regions of two of the actually fabricated PACs, one with AR = 3 and one with AR = 9. As can be noted, the produced pillar arrays are defect free and appear perfectly ordered to the eye. A closer inspection reveals that the maximum deviation between the drawing on the mask and the final spacings on the fabricated device was of the order of some 120 nm (average deviation on the order of some 70 nm). These deviations are smaller than the shift in sidewall distance (600 nm) deliberately imposed in the present study.

In Fig. 3, the camera images and intensity profiles of some of the injected coumarin dye bands are shown. After being loaded into the injection bands, the bands are carried along with the mobile phase and enter the PAC via a diverging flow distributor. For AR = 3, there is a clear warp for both studied dimensions, while for AR = 9 no difference is visually observed and straight band profiles are obtained for both values of the sidewall distance. The AR = 2.6 mm sidewall combined with the AR = 3 channel even leads to a reversal of the warp.

From the observations made in Fig. 3, one can conclude that, whereas the AR = 3 columns is clearly affected by a mismatch in the sidewall distance, whereas the dispersion in the AR = 9 columns is virtually insensitive to this mismatch.

3.2. Phenomenological explanation

Fig. 4 has been added to provide a phenomenological explanation for this observation. Comparing first the tortuous flow path
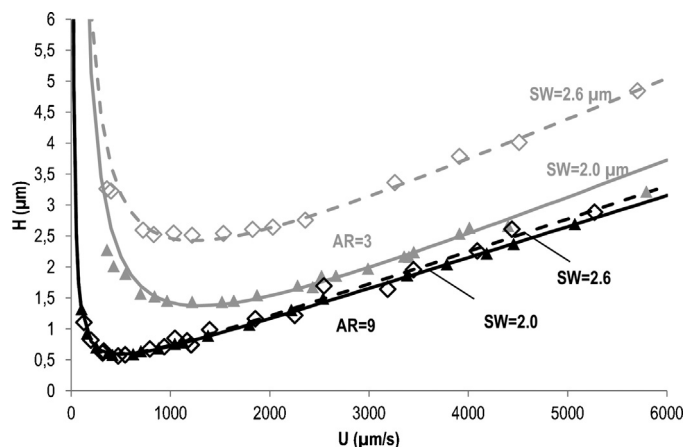

Fig. 5. van Deemters curves of C440 in MeOH (0.2 mM) as measured in the four different PACs (AR = 3 and 9, each combined with sidewall distances of 2.0 and 2.6 μm). The lines are van Deemter fits ($H = A + B/u + Cu$, with H the plate height, A, B and C constants and u the linear velocity).

(trajectory A) which is followed by the fluid in the center of the bed of the high AR pillars (Fig. 4b) with that followed by the fluid near the sidewall (trajectory B), and comparing the relative fraction of solid walls (determining the flow resistance) experienced by the flow, it can readily be noted that the difference between both trajectories is relatively small. The majority of both trajectories is composed of the mainly radially oriented tracks alongside the pillars (trajectory segments 1), while only a relatively small part of the trajectory is elapsed purely axially (trajectory segments 2). This segment is also the only part where a difference between trajectory A and B can be expected, as the sidewall trajectory experiences more solid wall per volume of liquid than the central bed trajectory, i.e., the specific surface in circle A is inevitably different from that in circle B, and also the local velocity in both circles will be different (flow rate through circle A is approximately double that of the flow rate through circle B), and in A the through-pore has a width of 3 μm, whereas it has a width of 2 μm in circle B. All these differences inevitably lead to a difference in local flow resistance, and hence to a different migration speed.

The main advantage of the high AR pillars now becomes readily apparent when considering that the circles A and B take up a considerably larger portion of the total trajectory for the small AR pillars (Fig. 4a) than for the large AR pillar case (Fig. 4b). As a consequence, it is evident that the sidewall distance has a bigger effect on the flow (mal)distribution.

3.3. Plate height measurements

To study the observations made in Section 3.1 in a more quantitative way, and to assess the influence of the mobile phase velocity, intensity profiles as the ones shown in Fig. 3 were collected for a wide range of mobile phase velocities. The corresponding peak widths were subsequently transformed into plate height values, which were subsequently plotted in the form a van Deemter curve (Fig. 5). It is striking to note that the curves for the two sidewall-cases nearly perfectly overlap for the AR = 9 case, while they differ strongly for the AR = 3 case, hence confirming the observations made in Fig. 3 over a broad range of velocities and corroborating further the hypothesis made in Section 3.2. The obtained minimum for the AR = 3 columns increases from a H = 1.5 μm for the near-optimal SW-design (SW = 2.0 μm) to 2.5 μm for the non-optimal SW-design (SW = 2.6 μm). This upward shift is maintained over the entire C-term dominated regime (velocity range above curve minimum), showing the inherent sensitivity of the AR = 3 design to a
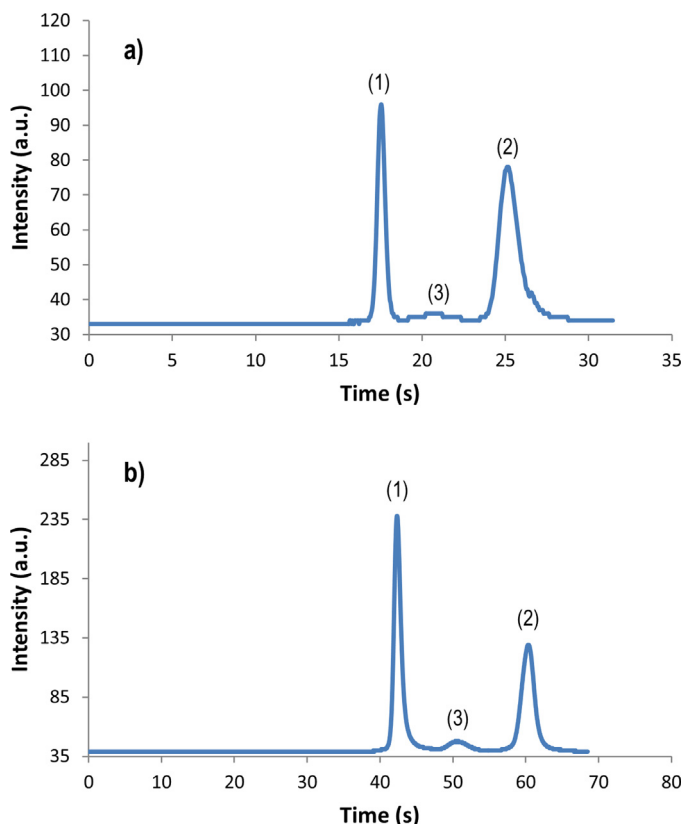
Fig. 6. Chromatograms of C440 (1) and C480 (2) + the typical ghost peak present in most C480 dyes (3) eluted with a mobile phase 60/40 (v/v) water/methanol and measured 5 mm downstream the injection zone with a sidewall distance SD: 2.0 μm for (a) AR = 3, H(C440) = 1.5 μm, H(C480) = 5.2 μm, mobile phase velocity: 0.29 mm/s, (b) AR = 9, H(C440) = 0.6 μm, H(C480) = 1.9 μm, mobile phase velocity 0.11 mm/s.

sidewall fabrication error. The much more tortuous flow paths in the AR = 9 are clearly much less (or even not) influenced by the sidewall design, given the near-perfect overlap of the SW = 2.0 μm and the SW = 2.6 μm curves.

To demonstrate that the band also remains straight under retained conditions, Fig. 6 shows the intensity profiles of the separation of two coumarin dyes in a channel with AR = 3 and AR = 9 under mild (to avoid overloading effects) retentive conditions. As can be noted from the plate height values cited in the caption, the AR = 9 channel produces plate heights that are about 2.5–3 times smaller than in the AR = 3 column. With the bad sidewall distance, the plate heights were even much larger, and furthermore did not remain constant because of the progressing sidewall effect contribution.

Undoubtedly, the suppression of the band broadening caused by the use of radially elongated particles does not only work in etched columns but also in 3-D columns packed with radially stretched particles, provided one could find a way to magically pack them all in the same direction.

4. Conclusions

Using two different degrees of pillar aspect ratios, combined with two different sidewall distances, it could be demonstrated that radially elongated PACs with a large AR are much more forgiving to a deviation from the ideal sidewall distance than small AR PACs. Technologically, this constitutes a huge advantage because small deviations (order of 100 nm) between the set and the finally achieved value for the inter-pillar distance are very common using mid-UV lithography based etching processes. A phenomenological explanation based on the smaller relative contribution of the zones with a deviating solid surface to mobile phase volume and a deviating local velocity to the total trajectory of the liquid has been given to explain the observations.

Acknowledgements

References

[1] B. He, N. Tait, F.E. Regnier, Fabrication of nanocolumns for liquid chromatography, Anal. Chem. 70 (1998) 3790–3797.
[2] F.E. Regnier, Microfabricated monolithic columns for liquid chromatography, J. High Resol. Chromatogr. 23 (2000) 19–26.
[3] B.E. Slentz, N.A. Penner, F.E. Regnier, Geometric effects of collocated monolithic support structures on separation performance in microfabricated systems, J. Sep. Sci. 25 (2002) 15–17.
[4] W. De Malsche, H. Eghbali, D. Clicq, J. Vangelooven, H. Gardeniers, G. Desmet, Pressure-driven reverse-phase liquid chromatography separations in ordered non-porous pillar array columns, Anal. Chem. 79 (2007) 5915–5926.
[5] L.C. Taylor, N.V. Lavrik, M.J. Sepaniak, High aspect ratio silicon oxide-enclosed pillar structures in microfluidic liquid chromatography, Anal. Chem. 82 (2010) 9549–9556.
[6] C. Aoyama, A. Saeki, M. Noguchi, Y. Shirasaki, S. Shoji, T. Funatsu, J. Mizuno, M. Tsunoda, Use of folded micromachined pillar array column with low-dispersion turns for pressure-driven liquid chromatography, Anal. Chem. 82 (2010) 1420–1426.
[7] Y. Song, M. Noguchi, K. Takatsuki, T. Sekiguchi, J. Mizuno, T. Funatsu, S. Shoji, M. Tsunoda, Integration of pillar array columns into a gradient elution system for pressure-driven liquid chromatography, Anal. Chem. 84 (2012) 4739–4745.
[8] L. Sainiemi, T. Nissila, R. Kostiainen, S. Franssila, R.A. Ketola, A microfabricated micropillar liquid chromatographic chip monolithically integrated with an electrospray ionization tip, Lab Chip 12 (2012) 325–332.
[9] K.B. Mogensen, F. Eriksson, O. Gústafsson, R.P.H. Nikolajsen, J.P. Kutter, Pure-silica optical waveguides, fiber couplers, and high-aspect ratio submicrometer channels for electrokinetic separation devices, Electrophoresis 25 (2004) 3788–3795.
[10] X. Illa, W. De Malsche, H. Gardeniers, G. Desmet, A. Romano-Rodríguez, Experimental study of the depth influence on the band broadening effect in a cyclo-olefin polymer column containing an array of ordered pillars, J. Chromatogr. A 1217 (2010) 5817–5821.
[11] N. Vervoort, J. Billen, P. Gzil, G.V. Baron, G. Desmet, Importance and reduction of the sidewall-induced band-broadening effect in pressure-driven microfabricated columns, Anal. Chem. 76 (2004) 4501–4507.
[12] J. Op De Beeck, W. De Malsche, S.T. Tezcan, P. De Moor, C. Van Hoof, G. Desmet, Impact of the limitations of state-of-the-art micro-fabrication processes on the performance of pillar array columns for liquid chromatography, J. Chromatogr. A 1239 (2012) 35–48.
[13] W. De Malsche, J. Op De Beeck, S. De Bruyne, H. Gardeniers, G. Desmet, Realization of 1 × 10^6 theoretical plates in liquid chromatography using very long pillar array columns, Anal. Chem. 84 (2012) 1214–1219.
[14] M. Callewaert, J. Op De Beeck, K. Maeno, S. Sukas, H. Thienpont, H. Ottevaere, H. Gardeniers, G. Desmet, W. De Malsche, Integration of uniform porous shell layers in very long pillar array columns using electrochemical anodization for liquid chromatography, Analyst 139 (2014) 618–625.
[15] J. Op De Beeck, M. Callewaert, H. Ottevaere, H. Gardeniers, G. Desmet, W. De Malsche, On the advantages of radially elongated structures in microchip-based liquid chromatography, Anal. Chem. 85 (2013) 5207–5212.